Design of CSP plants with optimally operated thermal storage

E. Casati [a,b,*], F. Casella [c], P. Colonna [a]

[a] *Propulsion & Power, Delft University of Technology, Kluyverweg 1, 2629 HS Delft, The Netherlands*
[b] *Dipartimento di Energia, Politecnico di Milano, via Lambruschini 4, 20156 Milano, Italy*
[c] *Dipartimento di Elettronica, Informazione e Bioingegneria, Politecnico di Milano, Piazza Leonardo da Vinci 32, 20133 Milano, Italy*

Received 16 June 2014; received in revised form 25 February 2015; accepted 16 March 2015

1. Introduction

Evolving towards a society not depending on fossil fuels is becoming a matter of the greatest interest, as it is increasingly clear that the current energy consumption and generation trend is not sustainable, due to the exhaus-tion of fossil fuel resources and its effects on climate change (Mediavilla et al., 2013; Galiana and Green, 2009). Devices to convert concentrated solar energy into useful work have been designed for over a century (Pifre, 1882; Francia, 1968; Spencer, 1989). The oil crisis triggered substantial R&D on solar energy conversion, and pilot plants were

* Corresponding author at: Propulsion & Power, Delft University of Technology, Kluyverweg 1, 2629 HS Delft, The Netherlands.
E-mail address: e.i.m.casati@tudelft.nl (E. Casati).

Nomenclature

Q, W	thermal and electrical power (various units)
m, P	mass flow rate ($kg\,s^{-1}$), electricity price ($\$\,kW\,h_{el}^{-1}$)
t, Rev	time (various units), plant yearly revenue ($M\$\,year^{-1}$)
T, x	temperature (°C), storage level (–)
η, α	efficiency and absorptivity (–)
$\epsilon_{avail}, \epsilon_{refl}$	average heliostats availability and reflectivity (–)
A, H	surface (m^2), height (m)
D, h_{TES}	diameter (m), storage capacity (eq. full-load hours)
loc	plant location (-)

Subscripts and superscripts

el, th	electric, thermal
REC, TOW	receiver, tower
def	defocusing
TES-C, TES-H	cold and hot tanks in the TES system
in, out	inlet and outlet conditions of a given HTF stream
opt, Inc., av	optical, incident (radiative flux), available
min, max	minimum and maximum
in, fin	initial and final

Acronyms (possibly used also as subscripts)

R&D	research and development
CSP	concentrated solar power
TES	Thermal Energy Storage
CR	central receiver (i.e., solar tower)
HTF	heat transfer fluid
PPA	power purchase agreement
TOD	time of day
LCOE	levelized cost of electricity
SAM	System Advisory Model
DNI	Direct Normal Irradiation ($W\,m^{-2}$)
NLP	non-linear programming
PB	power block
SF	solar field
SM	solar multiple
O&M	operations and maintenance
NPV	net present value

built during the 1980s. In recent years, renewed interest in concentrated solar power (CSP) plants has sparked a new surge in investments; in 2011 the power capacity of the CSP plants that were operational worldwide totalled 1.3 GW_{el}, that of plants under construction amounted to 2.3 GW_{el}, while that of planned plants added up to 31.7 GW_{el} (Pitz-Paal et al., 2013). A very relevant advan-tage of CSP power plants compared to other renewable energy conversion options is that the installation can inte-grate a comparatively inexpensive Thermal Energy Storage system (TES), enabling power to be generated when the sun is not shining, and contributing to their distinctive ability to provide dispatchable electricity. Recent research aimed at quantifying the added values of CSP dispatchability, the key findings being: (i) the dispatchability of CSP adds quantifiable economic benefits, (ii) the flexibility of CSP can aid the integration in the grid of other renewable energy technologies, such as solar photovoltaics (Denholm and Mehos, 2013).

Among the available CSP technologies, those based on linear collectors (i.e., parabolic troughs and Fresnel reflectors) and central receivers (CR, also known as solar towers) moved at the forefront in the last years. State-of-the-art plants use molten salts as working medium in the storage subsystem, which provides several hours of nominal operation without solar radiation. Commercial CR systems using molten salts as the working fluid in the solar receiver as well, i.e., implementing the so-called direct TES concept, have been recently deployed. This will be considered as the technology of choice in the present work but, notably, the presented methodology can be readily extended to other CSP technologies. The schematic layout of the first plant of this type, operating in Spain since 2011, is shown in Fig. 1.

The storage unit completely decouples the power block from the variable solar energy source, which is beneficial for both plant efficiency and reliability: in order to achieve better overall performance during the day, the control techniques for CSP systems usually aim at maintaining the solar receiver outlet temperature close to its nominal value, by varying the heat transfer fluid (HTF) mass flow rate. However, in the absence of significant energy storage, the operating point of the power block needs to follow the variations of the solar radiation, as discussed by Camacho et al. (2007a,b). On the contrary, the integration of a direct TES system into the power plant allows to use an additional control variable, i.e., the mass flow rate from the storage tank to the primary heat exchanger (steam gen-erator). Thus, the receiver outlet temperature and the power delivered to the conversion cycle can be controlled independently. This makes it possible to sustain constant power output during short transients (e.g., clouds passage), or to shift the production to better meet variable-price tariffs.

In the present work, according to a scheme currently adopted mainly in the USA, the produced electricity is supposed to be sold to a utility company at the previously negotiated power purchase agreement (PPA) bid price, multiplied by time-of-day (TOD) factors pre-defined by the applicable tariff, which account for the higher value

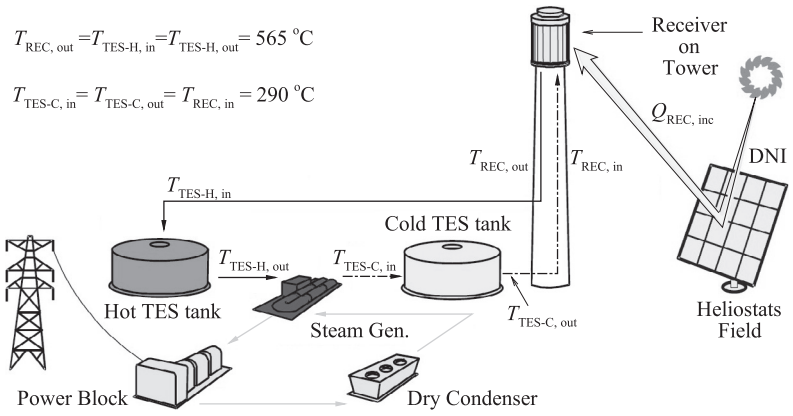

Fig. 1. Schematic layout of the Gemasolar 20 MW_{el} solar tower plant, capable of 15 h of full-load off-sun operation thanks to the storage system, adapted from Pacheco et al. (2002). The main simplification adopted here is also made explicit (see Section 2).

that the produced power has during peak hours. The PPA price is thus negotiated by the producer in order to balance the investment and operational costs, and hopefully make a profit. Both the tariff and the PPA price are assumed to be valid for the duration of the investment life which, in the subsequent analysis, is equal to 20 years (see Appendix B). For a detailed description of the PPA approach and how this allows to overcome the shortcomings of the other commonly adopted metric, i.e., the leve-lized cost of electricity (LCOE), the interested reader is referred to the works of Prior (2011) and Richert et al.(2012).

The availability of a TES system coupled with variable energy prices demands for an optimized operation of the plant, maximizing the revenues by exploiting the TES ability to shift the production to higher priced time slots. This problem has been considered by many authors in recent times, see, e.g., García-Barberena et al. (2012), Powell et al. (2012), Nolteernsting et al. (2012). With reference to real-time operation, Wittmann et al. (2008a) discuss the potential of weather forecast-based operation of CSP plants, stressing the importance of forecast quality. Wittmann et al. (2008b, 2011) present a methodology to maximize the revenues for a plant operating in a free energy market; the CSP plant is run with a price-driven strategy and, based on electricity pricing and weather forecasting, an economically optimized bidding strategy for the day-ahead energy market is determined. The authors identify a period comprising the next one or two trading days as a reasonable optimization horizon, considering the trade-off between profit gain and forecast quality. More recently, Lizarraga-Garcia et al. (2013) assessed the potential of a solar-thermal generation system in a fluctuating electricity prices context, by considering the innovative CSP technol-ogy proposed by Slocum et al. (2011). Biencinto et al.(2014) investigated the influence of the operation strategy, focusing on the charge/discharge process for a thermocline storage, on the yearly production of a parabolic trough CSP plant.

The research work documented here stems from the need of generalizing the analysis on optimized dispatching strategies for CSP plants, by considering the whole design-space of present-days systems, e.g., in terms of storage capacity and solar multiple. Furthermore, a novel assessment of how different control procedures can influence the design of the plant and the financial performance of the project is presented.

When a new CSP plant is being considered for construction at a specific location, models and tools are needed to assess the potential of eneregy production, and thus eventually compute the PPA price level that can repay for the investment within the specified time. A widely adopted, publicly available software tool for this purpose is the System Advisory Model (SAM) (Wagner, 2008; Turchi and Wagner, 2012; Wagner and Gilman, 2011), which is assumed as a reference in this work. The TES control strategy assumed by SAM is such that, for each hourly interval of operation, the controller tries to use all the available thermal power from the solar field (SF) and from the TES to drive the power block at the maximum possible load. This strategy is clearly sub-opti-mal when the TOD factor shows significant variations during peak hours, so it can be safely assumed that the plant being evaluated will eventually be operated using some kind of optimal control that will try to maximize the economic revenue by exploiting the available storage instead of the strategy assumed by SAM. In order to make correct decisions in terms of plant sizing and design would be therefore advantageous to include optimal con-trol even at this very early stage.

To this end, the method presented here is based on a dynamic model of the plant, replicating the basic modeling assumptions of the SAM software, which is then employed to formulate and solve a dynamic optimization problem in order to give a credible estimation of the potential of a future CSP plant, assuming optimal control is used for its operation. As the full details of the real-time implementation of the optimal controller cannot be available at this

very early design stage, it is reasonable to consider an idealized set-up of the control problem, assuming perfect matching between the model and the plant dynamics, and perfect knowledge of the future solar irradiation. The attained performance represents therefore the theoretical limit of the operation of a real-time optimal controller, which in reality will have to face modeling errors, unmodeled disturbances, and uncertain weather forecasts. Although the obtained results will be slightly optimistic, they will represent controlled plant operation in a much more credible way than those obtained with the short-sighted control policy usually assumed. Modern object-oriented languages and tools are used in order to concisely formulate and solve the optimal control problem with minimal implementation effort.

The main goal of the work is to show that, by means of these techniques and tools, the noteworthy advantages offered by optimal operation procedures can be easily unveiled and taken into account during the earliest design stages. The paper is structured as follows. The CSP plant model, replicating the main features of the SAM model, is introduced in Section 2. The reference control strategy and the optimal control problem are formulated in Section 3. The computational infrastruc-ture is discussed in Section 4, while the main results are presented and discussed in Section 5. Section 6 illus-trates the main conclusions and an outlook to future work.

2. Modeling framework

The CSP plant selected as a test case is a state-of-the-art 100 MW_{el} molten salts plant with direct storage, whose schematic layout is shown in Fig. 1. The general modeling framework closely follows the one used by SAM, as described in Wagner and Gilman (2011), therefore the following main simplifying assumptions hold:

1. The HTF temperature at the receiver outlet is assumed to be always kept at its nominal value $T_{REC,out}$. Also the temperature of the HTF exiting the steam generator, i.e., $T_{TES-C,in}$, is assumed to be constant within the considered operating range. The heat losses in the piping are neglected, leading to the equalities $T_{REC,out} = T_{TES-H,in}$ and $T_{REC,in} = T_{TES-C,out}$. Furthermore, also the storage tanks are supposed to be adiabatic, since the hourly thermal losses are negligible if compared to the stored energy, and their influence vanishes being the time horizon of the analysis of the order of few days. As a consequence $T_{TES-H,in} = T_{TES-H,out}$, and $T_{TES-C,in} = T_{TES-C,out}$, and only two temperature levels are present in the system model, as indicated in Fig. 1;
2. The dynamic behavior of thermal energy, determined for instance by thermal inertia effects, is explicitly modeled only in the TES tanks, since the (controlled) dynamics of the receiver system and power block is much faster;
3. The terms introduced to account for the thermal energy dynamics in the semi-steady framework of the SAM program have not been modeled: this is the case of the energy consumptions and time delays associated with the start-up and shut down of all the subsystems (Wagner and Gilman, 2011);
4. The temperature dependency of the thermodynamic properties of the HTF, i.e., density and specific heat, is neglected;
5. Perfect knowledge of future solar irradiation values is assumed, based on customarily adopted weather data files for the considered locations, such as those described in Wilcox and Marion (2008).

As shown in the following, these assumptions can enormously reduce the complexity of the design problem, while preserving the consistency of the results with respect to a corresponding omni-comprehensive SAM model.

For simplicity and numerical robustness, all the power variables are normalized to the nominal power block thermal power, all the mass flow rate variables to the corresponding mass flow rate, and the TES tank level to its nominal height. Notably, following the above men-tioned assumptions and simplifications, the equalities $m_{PB} = Q_{PB}$ and $m_{HTF} = Q_{HTF}$ hold, relating the circulating mass flow rate of HTF through the power block and the receiver to the thermal power transferred within the same subsystems. Since the plant location has a dramatic influ-ence on its performance, two different sites are considered, namely Daggett (US-CA, latitude 34.9°, longitude −116.8°, average annual DNI 2791 kW h m^{-2}) and Almeria (ES, lat-itude 36.9°, longitude −2.4°, average annual DNI 2035 kW h m^{-2}). Daggett is among the locations featuring the highest average annual DNI levels on Earth, with pre-dominant clean sky conditions and limited variations throughout the year. Almeria, with approximately 2/3 the insolation found in Daggett, can be nonetheless consid-ered as a very favorable European site. The general design data considered, i.e., the variables which are fixed in this work, are collected in Table 1. The operating limits regard-ing the receiver and the power block are expressed in terms of minimum/maximum fractions (i.e., f^{min}/f^{max}) of the relative design values for the incident radiative power

Table 1
General design data adopted for the 100 MW_{el} solar tower system, after Turchi and Wagner (2012), Wagner (2008), Wagner and Gilman (2011). η_{PB} is the power block thermal efficiency, $\eta_{REC,th}$ and α_{REC} the receiver thermal efficiency and absorptivity, respectively. ϵ_{avail} and ϵ_{refl} refer to the heliostats availability and reflectivity, both values accounting for the average SF performance.

$W_{el,gross}$ (MW_{el})	115	η_{PB} (%)	40
α_{REC} (%)	94	$\eta_{REC,th}$ (%)	88
ϵ_{avail} (–)	0.99	ϵ_{refl} (–)	0.90
$f^{min}_{Q_{REC,inc}}$ (–)	0.25	$f^{max}_{Q_{REC,inc}}$ (–)	1.2
$f^{min}_{m_{PB}}$ (–)	0.25	$f^{max}_{m_{PB}}$ (–)	1
$f^{min}_{x_{TES}}$ (–)	0	$f^{max}_{x_{TES}}$ (–)	1

$Q_{REC,inc}$, and for the mass flow rate fed to the steam generator m_{PB}. Similarly, the maximum and minimum storage levels are referred to the height of the technically exploitable storage volume, i.e., $f_{x_{TES}}^{min} = 0$ typically does not corresponds to a completely empty tank, as a minimum level is always present for technical reasons.

Based on all the above mentioned assumptions, the system model contains a single dynamic equation, describing the state of charge of the TES, and several algebraic equations, describing the power block and the TES operation set points. The solar input can be defined in terms of the power available to the receiver $Q_{REC,inc,av}$ (i.e., the total radiative flux which may reach the receiver if the SF is fully focused) as

$$Q_{REC,inc,av} = DNI(t, loc) A_{SF} \eta_{opt}(t, loc, SF) \epsilon_{avail} \epsilon_{refl}. \quad (1)$$

In Eq. (1), the functional dependence of DNI and of the SF optical efficiency η_{opt} from the time-varying weather conditions (t), and from the plant location (loc), is made explicit. As anticipated, weather data in the TMY3 format, containing data for various locations with an hourly sampling, are considered in this paper. The value of η_{opt} is evaluated hourly as a function of the solar position but, as shown in Eq. (1), it is also dependent on the SF characteristics. The same is obviously true for the total reflective area A_{SF}.

The dimension of the SF can be better expressed in terms of the solar multiple (SM) value, that is, the ratio of the receiver design thermal output to the power block design thermal input. As the SM size is increased, there will be a growing number of hours throughout the year whereby the available solar power exceeds the power block design power. In these conditions, the TES system is used to harvest (part of) the exceeding energy, until defocusing (part of) the heliostats might become necessary. Thus, a techno-economic optimal combination of the SF size and of the storage capacity has to be determined for the given plant and location (Duffie and Beckam, 2006). In particu-lar, the solar power harvesting system constituted by the SF, the tower, and the receiver, is the most capital intensive part of any solar energy project, and its optimization is therefore critical for the minimization of the overall costs (Pitz-Paal et al., 2011; Turchi and Wagner, 2012; Behar et al., 2013). The SM is thus used as the key parameter in the following analysis, and four solar fields characterized by SM = 1.5, 2, 2.5, and 3.5 are designed for the same hypothetical plant, i.e., starting from the specifications reported in Table 1.

Apart for the nominal characteristic indicated by the SM, however, the detailed design of the components involved is necessary in order to define both A_{SF} and the $\eta_{opt}(t, loc, SF)$ relation appearing in Eq. (1). In the present work, the PTGen program available within SAM (Wagner, 2008; Wagner and Gilman, 2011), and based on the DELSOL3 code (Kistler et al., 1986; Garcia et al., 2008), is adopted to this end. Solar fields with a surround radi-ally-staggered layout are considered. Even though several other geometries have been proposed in the literature (Behar et al., 2013), this arrangement is chosen here for the sake of simplicity. Furthermore, mainly as a conse-quence of the fact that the selected locations feature almost the same latitude and similar irradiation levels, the same SF designs can be used for both locations, making the comparison more straightforward. The SF modeling assumptions adopted in this study, together with the resulting designs, are reported in Appendix A. Summarizing, since all the computations involved by Eq. (1) can be carried out off-line once the solar field has been designed, $Q_{REC,inc,av}$ is eventually computed as a known, time-varying input for the plant model.

Also the price of the produced electricity P depends on known hourly TOD factors, in turn determined by the selected tariff, on the hour of the day, on the day of the week, and on the season, according to

$$P = TOD(t)\ PPA. \quad (2)$$

The power actually reaching the receiver $Q_{REC,inc}$ may then be calculated as

$$Q_{REC,inc} = Q_{REC,inc,av} - Q_{def}, \quad (3)$$

where Q_{def} is the power dumped by defocusing heliostats, which is a control variable of the problem. The following (normalized) equations

$$Q_{REC,abs} = Q_{REC,inc} \alpha_{REC}, \quad (4)$$

$$Q_{HTF} = Q_{REC,abs} \eta_{REC,th}, \quad (5)$$

$$m_{HTF} = Q_{HTF}, \quad (6)$$

$$W_{PB} = m_{PB} \eta_{PB}, \quad (7)$$

$$h_{TES} \frac{dx_{TES}}{dt} = m_{HTF} - m_{PB}, \quad (8)$$

$$x_{TES}(0) = x_{TES,0}, \quad (9)$$

Complete the model. Eq. (4) gives the thermal power absorbed in the receiver $Q_{REC,abs}$ and Eq. (5) the power Q_{HTF} transferred to the HTF. Eq. (6) relates the mass flow rate of HTF through the receiver m_{HTF} to Q_{HTF}, while Eq.(7) establishes the relation between W_{PB} and m_{PB}, where the power block efficiency η_{PB} is constant. This assump-tion is not expected to alter the results significantly since, as found during preliminary analyses, the amount of electricity generated with the power block efficiency being lower than 90% of its nominal value is below 3% for all the reasonable plant configurations considered in the cho-sen locations. Finally, the differential Eq. (8) describes the dynamics of the TES system, where h_{TES} is the capacity of the storage tank in terms of hours of operation at nominal power block load. The corresponding initial conditions for the state variable are explicitly defined by Eq. (9).

Several constraints need to be enforced in order to ensure feasible operation, namely

$$Q_{\mathrm{REC,inc}} \leqslant f^{\max}_{Q_{\mathrm{REC,inc}}}, \tag{10}$$

$$0 \leqslant Q_{\mathrm{def}} \leqslant Q_{\mathrm{REC,inc,av}}, \tag{11}$$

$$0 \leqslant m_{\mathrm{PB}} \leqslant 1, \tag{12}$$

$$f^{\min}_{x_{\mathrm{TES}}} \leqslant x_{\mathrm{TES}} \leqslant f^{\max}_{x_{\mathrm{TES}}}. \tag{13}$$

The first inequality states the maximum power that can be handled by the receiver, calling for a partial defocusing of the heliostat field if the available power $Q_{\mathrm{REC,inc,av}}$ becomes too high; the defocused power Q_{def} (second inequality) is non-negative and less than the available power. The normalized flow rate of HTF to the power block is comprised between 0 and 1 per unit (third inequality), while the storage tank state of charge x_{TES} is limited between a lower and an upper bound. Furthermore, both the solar field thermal power $Q_{\mathrm{REC,inc}}$ and the power block HTF flow m_{PB} have a minimum operating load, and need to be turned off if the desired load level is lower than that. The first constraint is enforced by substituting $Q_{\mathrm{REC,inc,av}} = 0$ whenever $Q_{\mathrm{REC,inc,av}} \leqslant f^{\min}_{Q_{\mathrm{REC,inc}}}$, which is done as a pre-processing task. The second constraint is handled by introducing extra terms in the optimization problem, see Section 3.2.

The resulting model has two known, time-varying inputs $Q_{\mathrm{REC,inc,av}}(t)$ and $f_{\mathrm{TOD}}(t)$, and two control variables $m_{\mathrm{PB}}(t)$ and $Q_{\mathrm{def}}(t)$. The model is readily encoded using the equation-based, object-oriented language Modelica (Mattsson et al., 1998), see also Section 4 and Listing 1 in Appendix C.

3. Operation strategy

3.1. Reference operation strategy

The model described in Section 2 can be used to predict the performance of the considered solar tower plant when the reference operation strategy, defined following Wagner (2008) and Wagner and Gilman (2011) is applied. This approach aims at satisfying the nominal power cycle demand, by making use of the available resources, namely of the solar field (SF) and the TES system, in a prioritized order. A sequence of logical statements is used to determine whether the power cycle demand can be met with only the SF, or with the SF and the TES, always in this order, while ensuring that the operative constraints (Eqs. (10)–(13)) are satisfied. In other words, the algorithm aims at running the power block at the maximum possible load for every time step, defocusing the solar field when its output $Q_{\mathrm{REC,inc,av}}$ exceeds the sum of the nominal thermal power input of the power block and of the maximum storage charging rate that fulfills the capacity limits over a one-hour horizon. In this way, the values of the decision variables m_{PB} and Q_{def} are determined disregarding any information about the electricity price and of future availability of solar irradiation.

The SAM software approximates the differential–algebraic equations of the model by assuming that all variables are constant within each hour of operation, i.e., by using the forward Euler's method. As there is no feedback from x_{TES} to any other variable of the model, the forward and backward Euler's methods give the same results, only shifted by one time step, which is irrelevant when determining yearly revenues.

3.2. Optimal control

The model described in Section 2 can be adopted to assess the potential of an optimized operation strategy for the considered plant, aimed at maximizing the revenue deriving from the sold electricity. The control objective is an integral cost to be minimized over the integration interval from time t_{in} to t_{fin}, i.e.,

$$\min \int_{t_{\mathrm{in}}}^{t_{\mathrm{fin}}} -W_{\mathrm{PB}}P + c\left(\frac{\mathrm{d}u}{\mathrm{d}t}\right)^2 + gs(u - f^{\min}_{m_{\mathrm{PB}}})\,\mathrm{d}t. \tag{14}$$

The first term in the integral accounts for the normalized instantaneous revenue from the sale of electricity. The second term, with $c > 0$, is introduced to penalize fast changes and oscillations of the control variable, as well as repeated re-starts of the plant during the same day. This provision, which aims at avoiding stressful operating regimes for the power block, is implemented in order to coherently follow the approach programmed into SAM. The third term, with $g > 0$, is introduced to avoid power block operation below the minimum load, along with the additional constraints

$$u = m_{\mathrm{PB}} + s, \tag{15}$$

$$0 \leqslant s \leqslant u. \tag{16}$$

The free control variable u, which is the output of the dynamic optimization problem together with Q_{def}, is the unconstrained normalized value of the HTF flow to the power block, while s is a slack variable. If $u > f^{\min}_{m_{\mathrm{PB}}}$, the term is minimized by taking the lowest possible value of s ($s = 0$), so that $m_{\mathrm{PB}} = u$. Conversely, if $u < f^{\min}_{m_{\mathrm{PB}}}$, the term is minimized by taking the highest possible value of s ($s = u$), so that $m_{\mathrm{PB}} = 0$. The values of c and g are empir-ically chosen to be the smallest possible, which actually suc-ceeds at avoiding control oscillation, restarting of the power block in the same day, and operation below the min-imum load, while perturbing as little as possible the opti-mization of the first term, i.e., the economic revenue of the plant. An additional constraint might be added to obtain a specific value of the storage at the end of the oper-ational period; this can be instrumental in comparing the performance of the optimal control to that of the original control strategy on equal grounds. The above-described optimal control problem can be readily encoded using the Optimica language (Åkesson et al., 2010), an extension of Modelica that also allows to specify the control objective and the constraint equations, see also Section 4 and Listing 2 in Appendix C.

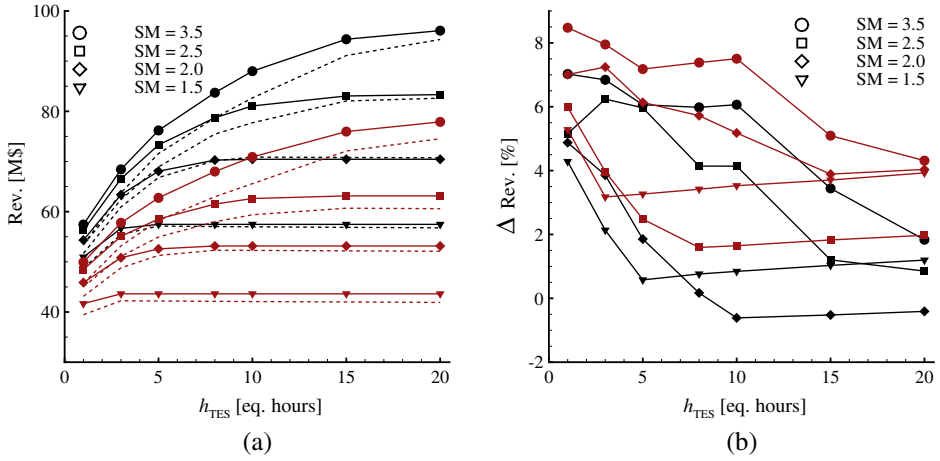

Fig. 2. Yearly simulation results in terms of revenue (Rev) as a function of TES system capacity (h_{TES}), for the two locations (Daggett: black lines, Almeria, red lines). The symbols refer to the SM values. (a) Comparison between the reference SAM model (dashed lines) and the Modelica model documented in this work (solid lines). (b) Percentage differences between the two models predictions.[1]

4. Computational infrastructure

The approach proposed in this work leverages on modern, high-level modeling languages for the problem formulation, and on software tools that automatically transform this description of the problem into low-level code that can be coupled with state-of-the-art numerical solvers. The model is encoded using the Modelica language (Mattsson et al., 1998; The Modelica Association, 2013), which is a high-level, non-proprietary, equation-based language for the modeling of systems described by differential–algebraic equations, while the optimization problem is encoded using the Optimica extension to the Modelica language (Åkesson, 2008). The Modelica/Optimica language is sup-ported by different tools, each implementing alternative strategies for the solution of the dynamic optimization problem (Modelon, 2013; OMCU, 2014).

The tool described in Modelon (2013) was used in the work described here. A collocation method was adopted in order to solve the problem (Andersson et al., 2011; Magnusson, 2012): the time-varying variables of the problem are approximated by Lagrange polynomials, that define the values of the variable in the optimization interval $t_{in} \leqslant t \leqslant t_{fin}$ as a direct function of the values at a finite set of nodal points, which become the unknowns of the prob-lem. In this way, the infinite-dimensional optimal control problem stated in Section 3.2 is transcribed into a finite-dimensional nonlinear programming (NLP) problem, which is then solved by an open-source NLP solver (Wächter and Biegler, 2006).

In order to directly compare the results with those obtained by the SAM program, which solves the differential equation by Euler's method, 0-order polynomials (i.e., piecewise constant functions) were used, with one-hour time intervals. It is worth pointing out that the proposed approach easily allows to use more accurate interpolations, simply by changing the set-up of the problem transcription. It is also easy to experiment with alternative solution strategies (e.g., multiple-shooting instead of collocation), as well as with different techniques to reduce the size of the NLP by means of symbolic manipulation, in order get the best performance in terms of convergence robustness and CPU time. In all these cases, the high-level formulation of the problem remains the same, only the choice of the tool and its configuration need to change, thus avoiding problem-specific low-level programming.

Last, but not least, the computational framework used to obtain the results presented in this paper has been entirely built using open-source software and open standards. It is then possible to use it as the foundation of extensions to publicly available tools such as the SAM program, without any issue that might arise from the use of commercial software.

5. Results and discussion

The first analysis aims at assessing the performance of the model developed in this work, see Section 2, by comparing its predictions to the yearly simulation results yielded by a reference SAM model (i.e., with all the main settings keeping their default values). The simulation is performed with a control algorithm emulating the SAM control strategy, see Section 3. The results are shown in Fig. 2(a), whereby the yearly revenue (Rev) is shown as a function of the TES system capacity h_{TES}, for several SM values, and for the two selected locations. Fig. 2(b) reports the percentage difference between the predictions of the developed models and those of the corresponding reference ones. Since several losses related to transient plant operation have been neglected, the simplified models tend to overestimate the plant performance. This misbehavior is accentuated for locations featuring a less regularly

[1] For interpretation of color in Figs. 2, 3, 4 and 5, the reader is referred to the web version of this article.

distributed solar resource, which in turn implies less steady operation, as exemplified here by the case of Almeria vs. Daggett. However, the discrepancies are acceptably low to deem the results significant and, notably, the largest deviations are encountered for plant layouts of negligible practical interest, i.e., those characterized by large solar fields and comparatively small storage capacity (see also Fig. 5). The adopted assumptions allow therefore to develop a comparatively simple model able to predict the relative differences of system performance with and with-out optimal control with reasonable accuracy in absolute terms. As expected, a large absolute difference in terms of potential plant revenue exists among Daggett and Almeria, as a consequence of the available solar input. However, a general trend can be identified, with the rev-enue increasing for larger SM values (larger solar fields) and, for a given SM value, growing as the size of the stor-age is increased, that is, as the amount of energy which needs to be dumped through defocusing is reduced.

On the other hand, a maximum revenue is reached for each SM value, beyond which an increase of h_{TES} does not influence further the revenue.

In order to provide a first insight, the results regarding a 10-days summer period in Daggett are presented in Fig. 3. The considered tariff was adopted by the utility company *Pacific Gas and Electric* in 2011, as defined in SAM (Wagner and Gilman, 2011). The observed system is char-acterized by a comparatively small storage capacity with respect to the field size. The time period starts with a week-end, which has a different f_{TOD} schedule. In order to perform the comparison on a fair basis, the initial and final state of the TES in the optimization problem are con-strained to be the same as they are in the simulation using the SAM control.

First of all, it can be noted from Fig. 3(a) that the use of optimal control allowed to increase the revenue of the period of about 7%, from 2.1 to 2.3 M$. The defocusing operation, envisaged in both cases, is managed differently,

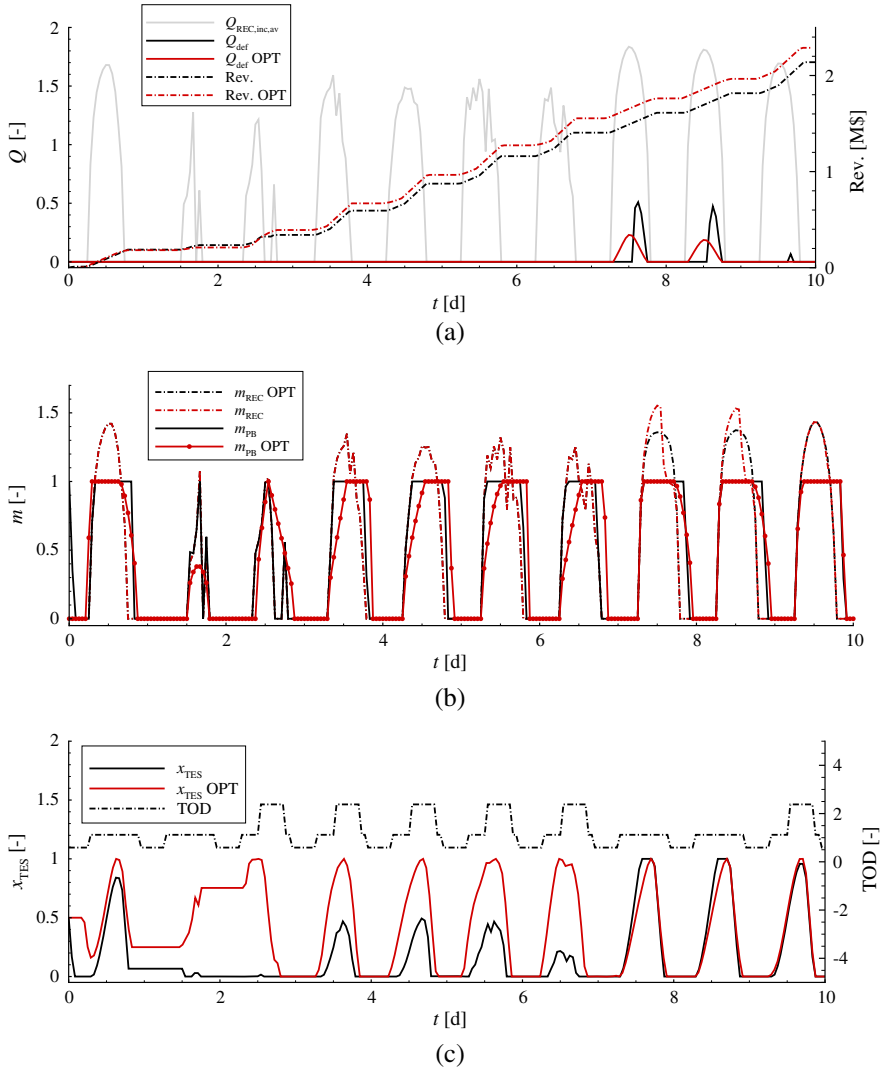

Fig. 3. Comparison between reference and optimized solar tower plant operation during a 10-days period in Daggett, from July the 7th to July the 16th. The considered system features solar multiple SM = 1.5 and storage capacity h_{TES} = 3 eq. hours.[1]

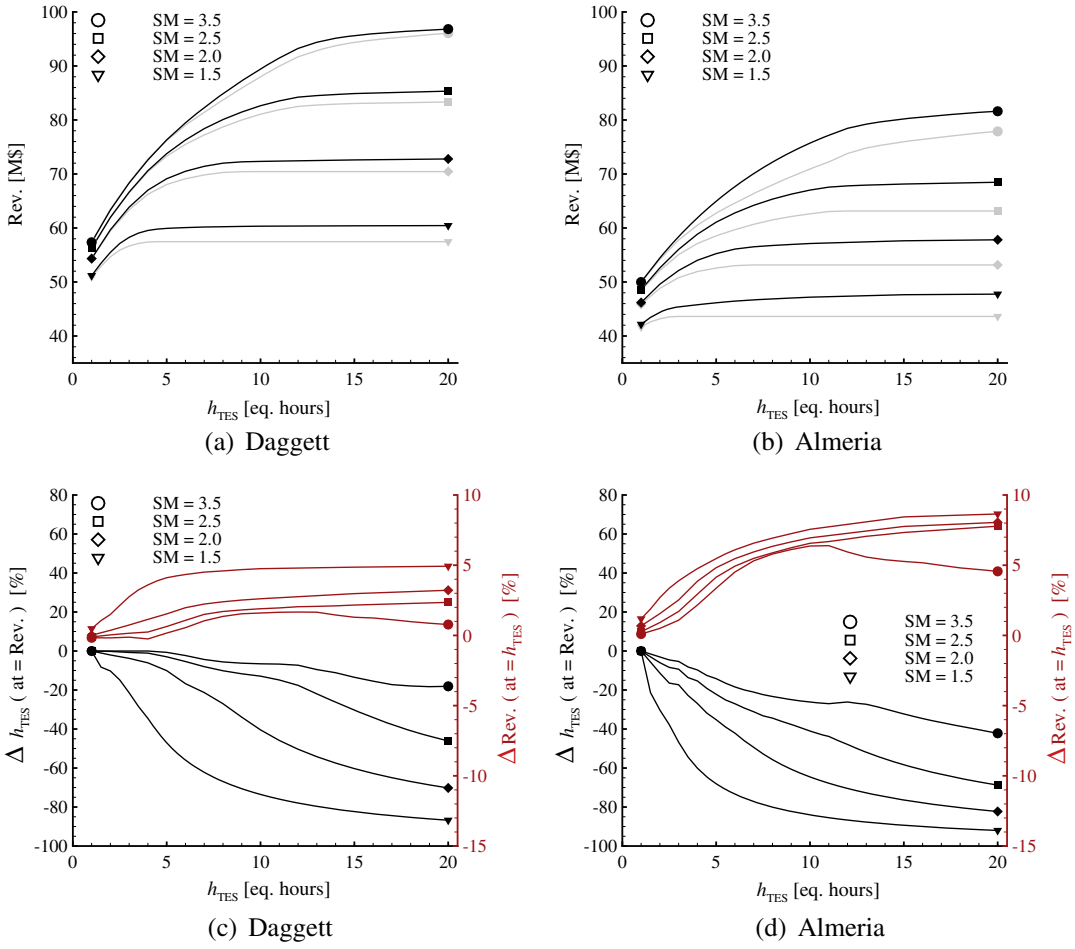

Fig. 4. Comparison between reference and optimized operation. (a) and (b) yearly revenue as a function of TES system capacity. Black lines: optimized operation, gray lines: reference operation. (c) and (d) percentage differences among the results in (a) and (b). Symbols refer to SM values.[1]

affecting the mass flow rate through the receiver, see, e.g., Fig. 3(b). The same graph shows how the power block operation varies as a consequence of the different control strategy. The effects of the optimized control strategy can be clearly understood by considering also Fig. 3(c), whereby both the storage level and the TOD factor are shown. Being the storage capacity comparatively small, the optimal controller cannot manipulate large amounts of energy, and the plant load profile is therefore similar in the two cases. However, the production tends to be shifted towards the afternoon hours of working days (when the TOD factor is highest), by reducing the load during off-peak hours, i.e., by limiting m_{PB} to a value sufficient to pre-vent storage overloading while avoiding the need of defo-cusing. Note that the hourly values of m_{PB}, represented by the red dots, never fall in the forbidden region between zero and the minimum load, as expected from the problem formulation. From the last three days shown in Fig. 3(c) can also be noted that, as the solar input becomes more regularly distributed during the day, the differences between the optimized operation and the reference one tend to vanish.

In order to present a thorough analysis, the yearly system performance is now considered. The solution strategy is the same, and the optimal control result has been obtained by separately optimizing each month of opera-tion, and then by summing the resulting monthly revenues. Since the adopted approach assumes perfect knowledge of the weather forecast within the analysis interval, consider-ing monthly intervals may seem inappropriate. However, as discussed by Wittmann et al. (2008b), expanding the forecasting horizon to more than 2–3 days has only a minor effect on the yearly revenue, since the storage capac-ity limitation constrains the amount of energy that the optimizer can shift.

The plant yearly revenue as a function of the storage capacity, with and without optimal control and for several SM values, is shown in Fig. 4(a) and (b).

Fig. 4(c) and (d) report the interpretation of these results in terms of percentage differences between the two operation strategies. The red lines (and red ordinates axis) provide the evaluation of the increase in revenue achievable thanks to the optimization. It can be appreciated how the optimal strategy, i.e., the black lines of Fig. 4(a) and (b),

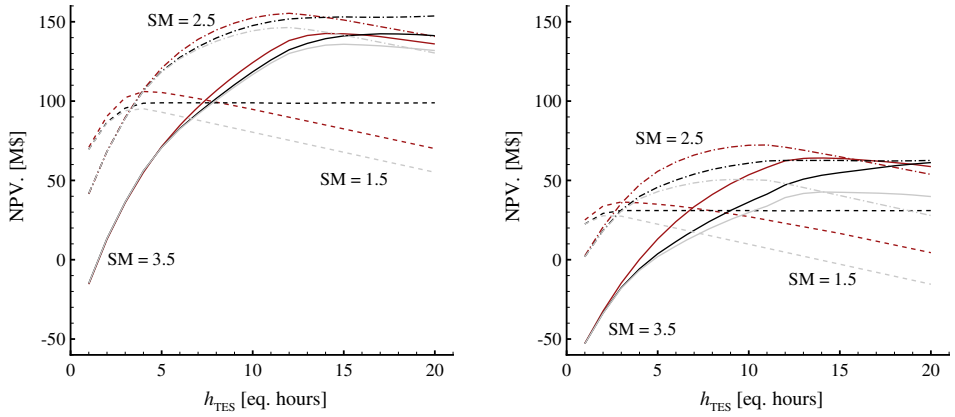

Fig. 5. Financial comparison between reference and optimized operation: NPV as a function of TES system capacity h_{TES}, for several SM values corresponding to different line formats (SM = 2.0 not reported for readability). Grey lines: reference control strategy; red lines: optimized strategy exploited to increase yearly revenue; black lines: optimized strategy exploited to decrease the investment.[1]

generally allows for a positive gain in terms of revenue with respect to the reference operation, i.e., the gray lines (in turn corresponding to the solid lines in Fig. 2(a)). This gain appears to be strictly related with the solar field size, which is a measure of the harvested solar energy, and with the TES capacity, in turn affecting how much of this energy can be manipulated by the optimizer to shift the produc-tion in time. The influence of the plant location is also evident and, as anticipated, the potential advantage is much larger when the solar resource distribution becomes less uniform, as is the case for Almeria. However, several common trends can be identified.

The curves are neatly ordered, with smaller solar fields yielding larger gains for a given TES capacity. This is an indication that the potential advantage offered by the optimizer, which allows to better allocate the available energy, gets relatively larger as such resource is less abundant, i.e., for smaller SM values. The curves originate from $\Delta Rev \approx 0$ for $h_{tes} = 1$, and are in general monotonically increasing with h_{tes} and concave down, and tend to saturate for large h_{tes} values. This is a consequence of the fact that, for a given SM value, there is a limiting h_{tes} over which addi-tional storage capacity cannot be exploited due to the solar input limitations: the production does not increase, see Fig. 4(a) and (a), and also the gain due to the optimizer tends to remain constant.

An interesting exception to this behavior is encountered for systems with large SM, which have the potential to behave as base load plants provided that the storage capacity is large enough. In this case the power block will tend to be run continuously, and the potential influence of the optimization will concurrently decrease. This is well represented by the SM = 3.5 curves, showing a clear point of inflection.

Notably, a complementary perspective can be considered, which aims at comparing the operating strategies for equal revenue yields, thus evaluating the potential reduction in TES system size they allow for, or, in other words, their impact on the system design. The result is shown by the black lines (and black ordinates axis). Also in this case, the gain achievable thanks to the optimization is considerable. As an example, one may consider a plant located in Almeria with SM = 2.5. For a TES capacity of 10 equivalent hours, such plant guarantees a revenue of 62.6 M $ when operated with a short-sighted strategy, as shown in Fig. 4(b). From the same figure, it can be deduced that the same revenue could be achieved with an optimally operated storage of significantly smaller size, i.e., namely, one with $h_{tes} \approx 6$ or, equivalently, 40% less capacity. This is exactly the result shown by the black line corresponding to SM = 2.5 in Fig. 4(d).

To put these conclusions in the right perspective, that is, in order to properly discriminate among an increase in the yearly revenue and a decrease of the capital cost, a financial analysis considering the whole plant life-time is necessary. A detailed financial model has been developed to this end, based on the framework implemented in SAM (Wagner and Gilman, 2011); the adopted methodolgy is detailed in Appendix B. All the considered plants are assumed to sell electricity at the same PPA price. The Net Present Value (NPV) of the project is adopted as the financial figure of merit, with the purpose of examining costs and revenues together, in order to evaluate mutually exclusive investment features and decisions, with positive NPVs representing profitable investments (Short et al., 1995).

The results of the analysis are summarized in Fig. 5, where the NPV is shown as a function of the TES system capacity, for several SM values. It can be immediately appreciated the dramatic difference in terms of profitability for the two locations. Also in this case, however, the main trends are common. It can be noted that all the gray curves, referring to the base case, i.e., to the reference control strategy, reach a maximum NPV value (NPV_{max}) for a given storage capacity value h_{TES}. Referring again to Fig. 2(a), such h_{TES} value is the one allowing to reach the maximum

revenue for the given SM value. In other words, this analysis allows to properly penalize solutions yielding the same revenue with an increasingly large investment.

The red curves show the impact of the optimal operating strategy on the project NPV, accounting for the revenue increase it allows for (see Fig. 4(c) and (d), red lines). It can be seen that the location of NPV_{max} in terms of h_{TES} is not varied with respect to the base case. In all cases, the financial advantage resulting from a complete analysis is larger than what predicted by considering the yearly revenues only. The SM = 2.5 case for Almeria can be considered as an example: NPV_{max} = 50.5 M$ for h_{TES} = 10 eq. hours is obtained for the base-case, i.e., the gray dash-dotted line in Fig. 5(b). For the same system, adopting the optimized control strategy allows for an yearly revenue increase of 6.5%, as shown in Fig. 4(d). However, this induces a gain of approximately 30.5% in terms of NPV, with NPV_{max} = 72.2 M$, as shown by the red dash-dotted line in Fig. 5(b).

The black curves account for the impact of the optimal operating strategy on the project NPV as well but, in this case, what is being evaluated is the potential for investment reduction (i.e., possible decrease of h_{TES} for a given rev-enue, see Fig. 4(c) and (d), black lines). As expected, the NPV is in general larger than the one characterizing the base-case and, for growing TES system capacities, may even become larger than in the previous case. However, these are solutions corresponding to systems of little prac-tical interest, as the maximum NPV for a given SM value is always reached when the optimizer is used to increase the revenue, i.e., by the red lines in Fig. 5. The factor determin-ing this situation is the comparatively low specific cost of the storage system which, for a state-of-the-art system with SM = 2.5 and h_{TES} = 10 eq. hours, accounts for approxi-mately 10% of the total installed cost. Even though these conclusions are influenced by the parameters adopted in the financial analysis, their validity is expected to hold under all the foreseeable realistic scenarios for state-of-the-art systems.

6. Conclusions

Concentrated solar power plants with thermal storage are a promising technology, increasingly considered as an option for widespread conversion of renewable energy. In a context of time-varying tariffs, the storage system can be used to shift the production to the most profitable hours, exploiting the dispatchability capabilities of this technology. The aim of the work presented here was to assess the potential of optimal control techniques, applied to the storage operation, to increase the profitability of the plant. To this end, the model of a state-of-the-art cen-tral receiver plant has been developed using high-level modeling languages, based on data available in the litera-ture and in the SAM reference software. Optimal control problems have then been formulated and solved. The dif-ferent operating strategies are compared based on a detailed financial analysis over the project life-time. A wide system design space is considered, and the results are presented for all the foreseeable combinations of solar field size and storage system capacity, for two representative locations.

A novel methodology is introduced, which allows to properly assess the potential of optimal control in terms of both the increased revenue and the reduced investment cost it allows for. In other words, it becomes possible to evaluate the influence of the operating strategy on the system design. It is demonstrated that optimal control should be taken into account when estimating the potential plant revenue since its design and sizing phase. This constitutes a new tool in the designer's hands who, depending on the specific project characteristics and financial framework, may be keen on favouring a larger electricity production or a comparatively lower investment cost. The main findings of the work are:

- For state-of-the art systems operating in a context of time-varying tariffs, it is always profitable to exploit optimal control to the end of increasing the plant revenue. On a yearly basis, average gains in revenue up to 10% are obtained with respect to usually adopted short-sighted strategies. However, these figures are amplified to gains up to 30% in terms of net present value of the investment when applying the complete financial analysis presented here. Notably however, the storage capacity for which maximum profitability occurs seems to be independent from the considered operating strategy.
- The potential of optimal control in terms of investment cost reduction, following the possibility of harvesting the same revenue with a smaller storage capacity, has been unveiled for the first time. However, for the considered scenarios, this solution is always suboptimal with respect to the maximization of revenue. This is mainly due to the comparatively low impact of the storage cost on the investment for current CSP systems, but might assume practical significance in evaluating plants with larger storage relative cost, as is the case of PV/batteries installations.
- The results have been obtained with open-source software, and a total of about 50 code lines.

A future step of this research might involve the implementation of the proposed methodology as an extension of reference design models, such as the model implemented into the SAM program.

Acknowledgements

This work has been carried out during E. Casati's research period at Politecnico di Milano, Dipartimento di Elettronica, Informazione e Bioingegneria, supported by the Dutch Technology Foundation STW, Applied Science Division of NWO and the Technology Program of the

Ministry of Economic Affairs, grant # 11143. The authors thankfully acknowledge the precious suggestions about JModelica.org from their colleagues at the University of Lund, Sweden: F. Magnusson, J.Åkesson, and C. Andersson. The help received by the NREL staff working on the SAM support forum, in particular by P. Gilman, has also been invaluable.

Appendix A. Solar fields design

This section details the procedure adopted in order to obtain the design of the solar fields considered here. It shows how the field reflective surface A_{SF} and its time-vary-ing optical efficiency η_{opt} are defined, see Eq. (1). As described in Section 2, several solar fields characterized by different SM values are designed for the same plant power output, for the locations of Daggett and Almeria, using the data reported in Table A.2. For a given SM value, the adopted algorithm, based on the DELSOL3 code (Kistler et al., 1986; Garcia et al., 2008), searches for a sys-tem design capable of yielding the highest financial returns, accounting for capital and other costs against the projected electricity production. The main objective of the tool is to optimize the geometric relationships among the main com-ponents of the solar power harvesting system, i.e., the solar field, the tower, and the receiver (Wagner, 2008). All the designed fields share the design boundaries defined by the data in Table A.2, aiming at reducing the complexity of the treatment and at facilitating the reproducibility of the results. The ranges of variation for the design variables have been selected such that reasonable layouts can be obtained regardless of the considered SM value.

The modeled receiver is of the tubular type, with con-stant absorptivity α_{REC} and emissivity $\epsilon_{coating}$. The main constraint regarding the design of this component is the maximum admissible heat flux on its surface (see "rec. max flux"). Regarding the solar field, a general layout con-straint is expressed in terms of the maximum/minimum dis-tance of the farther/closer heliostats row from the tower (see "helio.-tow. distance/H_{TOW}"). The modeled technol-ogy relies on square heliostats with a 12 m side (reflective part), whose main optical properties are also reported in Table A.2. As anticipated in Section 5, these are arranged in a *radially staggered, surround* field which, for the sake of the layout optimization, is discretized in radial and azi-muthal zones (see "N rad. zones" and "N azim. zones"). In order to solve the SF design problem, an optimal number of heliostats has to be allocated within each zone. The pro-gram evaluates discrete combinations of values for the main design variables, i.e., the diameter of the receiver D_{REC} and its height-over-diameter ratio $(H/D)_{REC}$, and the tower height H_{TOW}, with a grid-spacing based on the search interval and on the number of optimization levels (see "N opt. levels").

The most critical step is the evaluation of the flux distri-bution on the receiver surface as a function of solar posi-tion, which DELSOL3 calculates based on sophisticated aiming techniques. This information allows to iterate on the system design, accounting for the maximum flux levels the receiver can withstand, until an optimum layout is determined. The results regarding the geometry of the solar power harvesting system are reported in Table A.3. The radial step indicates the distance among two subsequent

Table A.3
Design results for the optimized solar power harvesting system. The adopted parameters and variables are listed in Table A.2.

	Solar Multiple (SM)			
	1.5	2.0	2.5	3.5
N_{helio} (–)	6435	8012	10,979	16,058
A_{SF} (m^2)	926,640	1,153,728	1,580,976	2,312,352
Total land area (km^2)	7.12	6.85	11.65	20.13
D_{REC} (m)	10.5	13	13	15.5
H_{REC} (m)	24.0	23.5	29.5	35.0
A_{REC} (m^2)	792	960	1205	1704
H_{TOW} (m)	144	189	189	211
Min dist. from tow. (m)	108	142	142	158
Radial step (m)	135	177	177	198
Max dist. from tow. (m)	1597	1558	2089	2534

Table A.2
Design parameters and variables used in the radially-staggered solar field layout optimization, with relative lower (LB) and upper (UB) bounds. Several quantities appeared in Table 1, and are reported here for the sake of clarity. For the three design variables, the range of variation is discretized into 10 points. These data are common to all the solar fields designed in this work.

Common parameters			
$W_{el,gross}$ (MW_{el})	115	η_{PB} (%)	40
α_{REC} (%)	94	$\epsilon_{coating}$ (–)	88
rec. max flux (kW_{th} m^{-2})	1000		
(helio. – tow. distance/H_{TOW})$_{min}$ (–)	0.75	(helio. – tow. distance/H_{TOW})$_{max}$ (–)	12
A_{helio} (m^2)	144	image error (mrad)	1.53
N rad. zones (–)	12	N azim. zones (–)	12
non SF land area (m^2)	182,109	SF land area multiplier (-)	1.3
N opt. levels (D_{REC}, $(H/D)_{REC}$, H_{TOW}) (–)	10		
Design variable	LB	UB	
D_{REC} (m)	8	30	
$(H/D)_{REC}$ (m)	0.5	2.5	
H_{TOW} (m)	100	300	

Table A.4
Design results for the optimized solar fields. Field optical efficiency η_{opt} (see Eq. (A.1)), calculated for the fields whose geometry is defined by the data in Table A.3. The results are reported, for the four solar multiples considered, as a function of Azimuth and Zenith angles.

Zenith (°)	SM	Azimuth (°)											
		0	30	60	90	120	150	180	210	240	270	300	330
0.5	**1.5**	.680	.680	.680	.680	.680	.680	.680	.680	.680	.680	.680	.680
	2.0	.720	.720	.720	.720	.719	.719	.719	.719	.719	.720	.720	.720
	2.5	.667	.667	.667	.667	.667	.667	.667	.667	.667	.667	.667	.667
	3.5	.640	.640	.640	.640	.640	.640	.640	.640	.640	.640	.640	.640
7	**1.5**	.680	.680	.679	.678	.678	.677	.677	.677	.678	.678	.679	.680
	2.0	.720	.720	.719	.716	.715	.714	.713	.714	.715	.716	.719	.720
	2.5	.669	.667	.666	.664	.664	.663	.663	.663	.664	.664	.666	.667
	3.5	.638	.638	.638	.637	.637	.637	.636	.637	.637	.637	.638	.638
15	**1.5**	.674	.673	.672	.669	.668	.666	.666	.666	.668	.669	.672	.673
	2.0	.714	.714	.710	.706	.703	.700	.699	.700	.703	.706	.710	.714
	2.5	.659	.659	.658	.656	.654	.653	.652	.653	.654	.656	.658	.659
	3.5	.632	.631	.631	.630	.629	.627	.627	.627	.629	.630	.631	.631
30	**1.5**	.659	.659	.656	.652	.647	.645	.643	.645	.647	.652	.656	.659
	2.0	.704	.702	.697	.688	.680	.674	.672	.674	.680	.688	.697	.702
	2.5	.646	.645	.642	.638	.635	.631	.631	.631	.635	.638	.642	.645
	3.5	.617	.616	.615	.612	.611	.609	.609	.609	.611	.612	.615	.616
45	**1.5**	.642	.641	.636	.630	.624	.619	.617	.619	.624	.630	.636	.641
	2.0	0.690	.687	.678	.666	.653	.646	.643	.646	.654	.666	.678	.687
	2.5	.627	.626	.622	.616	.610	.606	.605	.606	.611	.616	.622	.626
	3.5	.599	.598	.595	.591	.589	.586	.585	.586	.589	.593	.595	.598
60	**1.5**	.603	.600	.594	.585	.577	.570	.569	.572	.578	.585	.594	.600
	2.0	.646	.641	.630	.614	.599	.589	.585	.589	.600	.615	.631	.642
	2.5	.588	.585	.579	.572	.564	.558	.557	.559	.564	.573	.580	.586
	3.5	.560	.559	.556	.551	.546	.543	.543	.543	.547	.551	.556	.559
75	**1.5**	.480	.476	.469	.460	.448	.440	.440	.442	.450	.462	.470	.478
	2.0	.499	.494	.483	.464	.447	.432	.431	.434	.449	.466	.485	.496
	2.5	.464	.461	.454	.447	.436	.429	.428	.431	.437	.448	.457	.464
	3.5	.447	.445	.442	.436	.431	.426	.426	.428	.432	.438	.443	.448
85	**1.5**	.313	.308	.301	.294	.283	.275	.280	.278	.286	.299	.304	.311
	2.0	.296	.291	.282	.265	.255	.242	.244	.245	.257	.268	.286	.294
	2.5	.297	.294	.288	.281	.271	.265	.266	.267	.273	.283	.291	.297
	3.5	.292	.292	.290	.283	.278	.273	.275	.276	.281	.286	.292	.294

heliostats rows, and it is assumed constant within each field. It can be noted that the relation between the area A_{SF} and the SM value is not linear, reflecting the decrease of the optical performance as the solar field size grows. As detailed in Wagner (2008), DELSOL3 outputs also a 2D matrix reporting the field optical efficiency appearing in Eq. (1), and defined as

$$\eta_{opt}(t, loc, SF) = (\mathcal{F}_{REC} A_{REC})(DNI A_{helio} N_{helio})^{-1}, \quad (A.1)$$

where $\mathcal{F}_{REC}$ [kW_{th} m^{-2}] is the average flux incident on the receiver at the given time, and A_{REC} [m^2] is the receiver surface. In other words, the total radiation incident on the receiver is divided by the total radiation incident on the heliostat field mirrors for a given solar position. This last bit of information is fully specified in terms of Azimuth and Zenith angles which, in turn, can be calcu-lated for the given time of the year (t) and the plant loca-tion (loc) by means of standard methods, see, e.g., Duffie and Beckam (2006). The values of η_{opt}, calculated for the fields whose geometry is defined by the data in Table A.3, are reported in Table A.4. As anticipated, the results collected in Tables A.3 and A.4 are common for the selected locations, mainly as a consequence of the fact that Daggett and Almeria feature an almost equal latitude.

Appendix B. Financial analysis

The financial model presented here has been developed following the SAM framework (Wagner and Gilman, 2011) and the work of Short et al. (1995). The parameters for the analysis, reported in Table B.5, are assigned typi-cally encountered values, see, e.g., Turchi and Wagner (2012). The selected figure of merit is the Net Present Value (NPV) of the solar power project, i.e., the sum of the actualized net cash flows along the project life (Short et al., 1995), which reads

$$NPV = \sum_{n=0}^{N} \frac{F_n}{(1+d)^n} = F_0 + \frac{F_1}{(1+d)^1} + \frac{F_2}{(1+d)^2} + \cdots + \frac{F_N}{(1+d)^N}. \quad (B.1)$$

N is the analysis period (i.e., the project life), and d the nominal discount rate

$$d = ((1 + d_r/100)(1 + i/100) - 1) \cdot 100, \quad (B.2)$$

where d_r is the real discount rate, and i is the inflation rate. The F_n terms represent the net after-tax cash flows in the n years: a negative value represents a net outflow, a positive value a net inflow. They are evaluated as

$$F_n = \begin{cases} -(1 - f_{debt}/100)(DC + IC) & \text{if } n = 0 \quad (a) \\ \text{op. inc.}(n) - \text{inc. tax}(n) + \text{tax sav.}(n) & \\ -\text{debt repaym.}(n) - \text{debt int. paym.}(n) & \text{if } 0 < n \le N \quad (b) \end{cases} \quad (B.3)$$

For the first year of the analysis, i.e., conventionally the 0th year, the financial balance accounts for the debt portion of the investment only, expressed as a fraction f_{debt} of the total installed costs, i.e., as shown in Eq. (B.3a), the sum of direct-costs (DC) and indirect ones (IC), respec-tively defined as

$$DC = (SI + SF + BOP + PB + TES + TOW + REC)(1 + \text{contingency}/100), \quad (B.4)$$

$$IC = EPC + LC + S_{tax}. \quad (B.5)$$

The first two terms in Eq. (B.4) account for the solar field costs, in terms of site improvement SI and of heliostats cost SF, as $SI = A_{SF} SI_{coeff}$ and $SF = A_{SF} SF_{coeff}$, respectively. Similarly, BOP and PB account for the cost of the Balance Of Plant and of the power block, as $BOP = W_{el,gross} BOP_{coeff}$ and $PB = W_{el,gross} PB_{coeff}$. TES relates the storage system cost to its capacity in terms of thermal energy, i.e., $TES = W_{el,gross} TES_{coeff}$. The tower cost is evaluated by multiplying a fixed cost component to an exponential function of the tower height, i.e., $TOW = EXP(TOW_{scaling} H_{TOW}) TOW_{fixed}$. The receiver cost is found by multiplying the cost of a reference component (i.e., REC_{ref}) by the corresponding surface ratio, i.e., $REC = REC_{ref} (A_{REC}/A_{REC,ref})^{REC_{scaling}}$.

As shown in Eq. (B.5), the indirect costs account for the Engineering-Procurement-Construction Costs (EPC), calculated as a percentage r_{EPC} of the direct costs. The land cost term LC is evaluated by applying the unit cost coefficient r_{land} to the total land area needed (see Table A.3). The sales tax S_{tax} is a one-time tax included in the project total installed cost, and therefore in the depreciable basis (see in

Table B.5
Data adopted in the financial analysis. The meaning of the reported quantities is discussed in the body of the Appendix.

General							
N (year)	25	d_r (% $year^{-1}$)	8.2	i_{infl} (% $year^{-1}$)	2.5	N_{loan} (year)	20
f_{debt} (%)	50	r_{loan} (% $year^{-1}$)	8	$r_{inc.tax}$ (% $year^{-1}$)	40	r_{ITC} (% DC + IC)	30
Direct and indirect costs (Eqs. (B.4) and (B.5)*)*							
SI_{coeff} ($ m^{-2})	15	SF_{coeff} ($ m^{-2})	180	BOP_{coeff} ($ kW_e^{-1})	350	PB_{coeff} ($ kW_e^{-1})	1200
TES_{coeff} ($ kW h_t^{-1})	27	TOW_{fixed} (M$)	3	$TOW_{scaling}$ (–)	0.0113	REC_{ref} (M$)	110
$A_{REC,ref}$	1571	$REC_{scaling}$ (–)	0.7	contingency (%)	7	r_{EPC} (% DC)	11
r_{land} ($ m^{-2})	2.47	$r_{sales\ tax}$ (%)	5	$base_{sales\ tax}$ (% DC)	80		
Operating income (Eq. (B.6)*)*							
$O\&M_{cap,coeff}$ ($ kW_e^{-1})	65	$O\&M_{gen,coeff}$ ($ MWh_e^{-1})	4	$r_{insurance}$ (% DC + IC)	0.5	$r_{PPA,escalation}$ (% $year^{-1}$)	1
$r_{perf.degr.}$ (% $year^{-1}$)	0.5						

the following), and is calculated on a fraction of the direct costs as $S_{tax} = DC(base_{sales\ tax}/100)(r_{sales\ tax}/100)$.

Regarding the financing scheme, a fraction f_{debt} of the total installed cost is assumed to be borrowed. This initial debt is payed back through annual amounts (i.e., "debt repaym."), calculated by using the levelized mortgage payment methodology, i.e., by assuming constant payments on principal amount over the loan term N_{loan} at the rate r_{loan}. The payment of interests is evaluated by applying the same rate on the remaining debt, through annual amounts (i.e., "debt int. paym.").

For the calculation of the cash flows for the following years of the analysis, i.e., when $0 < n \leqslant N$, Eq. (B.3b) applies (the dependency from n, common to all terms, is not explicitly indicated in the following in order to improve readability). The first term accounts for the operating income the project generates in the nth year, i.e.,

$$\text{op.inc.} = \text{Rev} - (\text{O\&M}_{cap} + \text{O\&M}_{gen} + \text{insurance}). \quad \text{(B.6)}$$

Rev indicates the yearly revenue from sold electricity, i.e., for the 1st year, the performance indicator used throughout Section 5. Thus, an annual average value for the energy price $\overline{P}_E$ can be defined as $\overline{P}_E = E/\text{Rev}$, with E being the sold energy. These values are used as the basis for the analysis and, for the following years (i.e., for $1 < n \leqslant N$), the plant revenue is calculated as $\text{Rev} = E_{corr}/\overline{P}_{E,corr}$, whereby E_{corr} corrects E accounting, year after year, for the degradation of performance $r_{perf.degr.}$, and $\overline{P}_{E,corr}$ applies the annual PPA price escalation rate $r_{PPA,escalation}$ to $\overline{P}_E$. Furthermore, both quantities are yearly inflated by considering the i_{infl} rate.

The $\text{O\&M}_{cap}$ and $\text{O\&M}_{gen}$ terms in Eq. (B.6) refer to the operating and maintenance costs related to the plant nameplate power capacity and the generated energy E, and are evaluated by multiplying these quantities by the corresponding coefficients $\text{O\&M}_{cap,coeff}$ and $\text{O\&M}_{gen,coeff}$. Also the annual insurance cost is considered as an operating expense (therefore reducing the taxable income, see the following), and is calculated as a percentage $r_{insurance}$ of the total installed costs (i.e., DC + IC). For the years of the analysis following the first, all the quantities appearing between brackets in Eq. (B.6) are recalculated accounting for inflation.

The second term in Eq. (B.3b) refers to a global annual income tax, which applies to a percentage $r_{inc.tax}$ of the taxable income, and reads

$$\text{inc.tax} = (r_{inc.tax}/100)(\text{op. inc.} - \text{debt int. paym.} - \text{depreciation}). \quad \text{(B.7)}$$

The depreciation term represents the decrease in value of project assets over the analysis period, and it reduces the taxable income. In the present work, the so-called Modified Accelerated Cost Recovery System depreciation schedule offered by the US Federal government using a five-year life and half-year convention is used, commonly referred to as *5-yr MACRS* (Short et al., 1995). The depre-ciation is expressed as a percentage of the depreciable basis, corresponding to the total installed costs in this analysis, and it applies to the first five years of the project life as follows: 20%, 32%, 19.2%, 11.52%, 11.52%, and 5.76%.

The third term in Eq. (B.3b) refers to tax savings deriving from tax credits or incentives. In the present analysis, only an Investment Tax Credit equal to a fraction r_{ITC} of the initial investment (i.e., of the total installed costs) is

```
model CSP_tower
 input Real Q_rec_inc_av ;
 input Real m_PB;
 input Real Q_def;
 output Real x_TES;
 Real m_rec_HTF;
 Real Q_rec_inc;
 Real Q_rec_abs, Q_rec_HTF, Q_rec_HTF, Q_lost, W_PB;
 parameter Real alpha_rec = 0.94;
 parameter Real eta_rec_th = 0.88;
 parameter Real eta_des = 1;
 parameter Real f_max_Q_rec_inc = 1.2 ;
 parameter Real T_TES;
 parameter Real x_TES_0 = 0;
equation
 Q_rec_inc  = Q_rec_inc_av - Q_def;
 Q_rec_HTF  = Q_rec_abs * (1 - eta_rec_th);
 m_rec_HTF = Q_rec_HTF;
 W_PB       = m_PB * eta_des;
 T_TES * der(x_TES) = m_rec_HTF - m_PB;
initial equation
 x_TES = x_TES_0;
end CSP_tower;
```

Listing 1. Plant model in Modelica.

```
optimization optim(objectiveIntegrand =
  -plant.W_PB*f_TOD + c*du_dt^2 + g*s*(u-plant.f_min_m_PB),
  startTime = 0,finalTime = 7*24*3600);
 CSP_tower plant(T_TES=15*3600);
 parameter Real g = 1;
 parameter Real c = 2250000;
 // Known inputs
 input Real Q_rec_inc_av;
 input Real f_TOD;
 // Unknown control variables
 input Real f(min=0, free=true);
 input Real du_dt (free=true, nominal = 4e-5);
 // Other extra variables
 Real s(free=true);
 Real u(min=0,max=1.0);
equation
 Q_rec_inc_av  = plant.Q_rec_inc_av;
 TOD           = plant.TOD;
 u             = plant.m_PB + s;
 der(u)        = du_dt;
 f             = plant.Q_def;
initial equation
 plant.m_pb=0;
constraint
 s >= 0; s <= u;
 m_PB >= 0; m_PB <= 1;
 Q_def >= 0;
 x_TES >= 0; x_TES <= 1;
 Q_rec_inc >=0; Q_rec_inc <= f_max_Q_rec_inc;
 f >= 0; f <= plant.Q_rec_inc_av;
 plant.x_st(finalTime) = 0;
end optim;
```

Listing 2. Optimization problem in Optimica.

considered. This applies on the first year of the analysis, i.e., for $n = 1$ only.

Appendix C. Modelica and Optimica listings

See Listings 1 and 2.

References

Åkesson, J., 2008. Optimica – an extension of Modelica supporting dynamic optimization. In Proceedings 6th International Modelica Conference, Bielefeld, Germany, pp. 57–66.

Åkesson, J., Årzén, C., Gäfvert, M., Bergdahl, T., Tummescheit, H., 2010. Modeling and optimization with Optimica and JModelica.org – languages and tools for solving large-scale dynamic optimization problems. Comput. Chem. Eng. 34, 1737–1749.

Andersson, J., Åkesson, J., Casella, F., Diehl, M., 2011. Integration of CasADi and JModelica.org. In: Clauss, C. (Ed.), Proceedings 8th International Modelica Conference. Modelica Association, Dresden, Germany, pp. 218–231.

Behar, O., Khellaf, A., Mohammedi, K., 2013. A review of studies on central receiver solar thermal power plants. Renew. Sustain. Energy Rev. 23, 12–39.

Biencinto, M., Bayn, R., Rojas, E., Gonzlez, L., 2014. Simulation and assessment of operation strategies for solar thermal power plants with a thermocline storage tank. Sol. Energy 103, 456–472.

Camacho, E., Rubio, F., Berenguel, M., Valenzuela, L., 2007a. A survey on control schemes for distributed solar collector fields. Part I: modeling and basic control approaches. Sol. Energy 81, 1240–1251.

Camacho, E., Rubio, F., Berenguel, M., Valenzuela, L., 2007b. A survey on control schemes for distributed solar collector fields. Part II: advanced control approaches. Sol. Energy 81, 1252–1272.

Denholm, P., Mehos, M., 2013. Quantifying the value of CSP with thermal energy storage. In: SunShot Concentrating Solar Power Program Review 2013. U.S. Department of Energy (DOE).

Duffie, J., Beckam, W., 2006. Solar Engineering of Thermal Processes, third ed. John Wiley & Sons Inc.

Francia, G., 1968. Pilot plants of solar steam generating stations. Sol. Energy 12, 51–64.

Galiana, I., Green, C., 2009. Let the global technology race begin. Nature 462, 570–571.

García-Barberena, J., García, P., Sanchez, M., Blanco, M.J., Lasheras, C., Padrós, A., Arraiza, J., 2012. Analysis of the influence of operational strategies in plant performance using SimulCET, simulation software for parabolic trough power plants. Sol. Energy 86, 53–63.

Garcia, P., Ferriere, A., Bezian, J.-J., 2008. Codes for solar flux calculation dedicated to central receiver system applications: a comparative review. Sol. Energy 82, 189–197.

Kistler, B., 1986. A Users Manual for DELSOL3: A Computer Code for Calculating the Optical Performance and Optimal System Design for Solar Thermal Central Receiver Plants. Technical Report SAND86-8018 Sandia National Labs, Albuquerque, NM.

Lizarraga-Garcia, E., Ghobeity, A., Totten, M., Mitsos, A., 2013. Optimal operation of a solar-thermal power plant with energy storage and electricity buy-back from grid. Energy 51, 61–70.

Magnusson, F., 2012. Collocation Methods in JModelica.org. Master's Thesis Department of Automatic Control, Lund University.

Mattsson, S.E., Elmqvist, H., Otter, M., 1998. Physical system modeling with Modelica. Control Eng. Pract. 6, 501–510.

Mediavilla, M., de Castro, C., nigo Capellán, I., Miguel, L.J., naki Arto, I., Frechoso, F., 2013. The transition towards renewable energies: physical limits and temporal conditions. Energy Policy 52, 297–311.

Modelon, A.B., 2013. JModelica.org User Guide: Version 1.9.

Nolteernsting, F., Fischer, D., Gall, J., Abel, D., 2012. Optimal storage usage in CSP: a dynamic programming approach. In: Proceedings of the 18th SolarPACES conference. Marrakech, Morocco.

Open Source Modelica Consortium, 2014. OpenModelica Users Guide for OpenModelica 1.9.1 Beta2.

Pacheco, J. et al. 2002. Final Test and Evaluation Results from the Solar Two project. Technical Report SAND2002-0120 Sandia National Lab Albuquerque, New Mexico.

Pifre, A., 1882. A solar printing press. Nature 26, 503–504.

Pitz-Paal, R., Botero, N., Steinfeld, A., 2011. Heliostat field layout optimization for high-temperature solar thermochemical processing. Sol. Energy 85, 334–343.

Pitz-Paal, R., Amin, A., Bettzüge, M., Eames, P., Fabrizi, F., Flamant, G., Novo, F.G., Holmes, J., Kribus, A., van der Laan, H., Lopez, C., Papagiannakopoulos, P., Pihl, E., Smith, P., Wagner, H.-J., 2013. Concentrating solar power in Europe, the Middle East and North Africa: achieving its potential. J. Energy Power Eng. 7, 219–228.

Powell, K., Hedengren, J., Edgar, T., 2012. Dynamic optimization of solar thermal systems with storage. In: Proceedings of the AIChE 2012 Annual Meeting. Pittsburgh, PA.

Prior, B., 2011. Cost and LCOE by Generation Technology 2009–2020. <http://www.greentechmedia.com/images/wysiwyg/research-blogs/GTM-LCOE-Analysis.pdf> (accessed November 2013).

Richert, T., Riffelmann, K., Nava, P., 2012. LCOE versus PPA bid price – how different financing parameters influence their values. In: Proceedings of the 18th SolarPACES Conference. Marrakech, Morocco.

Short, W., Packey, D., Holt, T., 1995. A Manual for the Economic Evaluation of Energy Efficiency and Renewable Energy Technologies. Technical Report NREL/TP-462-5173 National Renewable Energy Laboratory, U.S. Department of Energy.

Slocum, A., Codd, D., Buongiorno, J., Forsberg, C., McKrell, T., Nave, J.-C., Papanicolas, C., Ghobeity, A., Noone, C., Passerini, S., Rojas, F., Mitsos, A., . Concentrated solar power on demand. Sol. Energy 85, 1519–1529.

Spencer, L., 1989. A comprehensive review of small solar-powered heat engines: Part I. A history of solar–powered devices up to 1950. Sol. Energy 43, 191–196.

The Modelica Association, 2013. Modelica – A Unified Object-Oriented Language for Physical Systems Modeling – Language Specification Version 3.2 Revision 2. <www.modelica.org> (last accessed June 2014).

Turchi, C., Wagner, M., 2012. Power tower reference plant for cost modeling with the system advisor model (SAM). In: Proceedings of the World Renewable Energy Forum, WREF 2012, vol. 4, pp. 2598–2605.

Wächter, A., Biegler, L.T., 2006. On the implementation of an interior-point filter line-search algorithm for large-scale nonlinear programming. Math. Program. 106, 25–57.

Wagner, M., 2008. Simulation and Predictive Performance Modeling of Utility–Scale Central Receiver System Power Plants. Master's Thesis University of Wisconsin Madison.

Wagner, M., Gilman, P., 2011. Technical Manual for the SAM Physical Trough Model. Technical Report NREL/TP-5500-51825 National Renewable Energy Laboratory, US Department of Energy.

Wilcox, S., Marion, W., 2008. Users Manual for TMY3 Data Sets. Technical Report NREL/TP-581-43156 National Renewable Energy Laboratory, US Department of Energy.

Wittmann, M., Breitkreuz, H., Schroedter-Homscheidt, M., Eck, M., 2008a. Case studies on the use of solar irradiance forecast for optimized operation strategies of solar thermal power plants. IEEE J. Sel. Topics Appl. Earth Observations Rem. Sens. 1, 18–27.

Wittmann, M., Eck, M., Hirsch, T., Pitz-Paal, R., 2008b. Theoretical economic potential of the Spanish premium tariff for solar thermal power plants. In: Proceedings of the 14th SolarPACES Conference. Las Vegas – CA, United States.

Wittmann, M., Eck, M., Pitz-Paal, R., Müller-Steinhagen, H., 2011. Methodology for optimized operation strategies of solar thermal power plants with integrated heat storage. Sol. Energy 85, 653–659.